Author/s:
Battlay, P;Craig, S;Putra, AR;Monro, K;De Silva, NP;Wilson, J;Bieker, VC;Kabir, S;Shamaya, N;van Boheemen, L;Rieseberg, LH;Stinchcombe, JR;Fournier-Level, A;Martin, MD;Hodgins, KA

Title:
Rapid Parallel Adaptation in Distinct Invasions of Ambrosia Artemisiifolia Is Driven by Large-Effect Structural Variants

Date:
2025-01-01

Citation:
Battlay, P., Craig, S., Putra, A. R., Monro, K., De Silva, N. P., Wilson, J., Bieker, V. C., Kabir, S., Shamaya, N., van Boheemen, L., Rieseberg, L. H., Stinchcombe, J. R., Fournier-Level, A., Martin, M. D. & Hodgins, K. A. (2025). Rapid Parallel Adaptation in Distinct Invasions of Ambrosia Artemisiifolia Is Driven by Large-Effect Structural Variants. Molecular Biology and Evolution, 42 (1), https://doi.org/10.1093/molbev/msae270.

Persistent Link:
https://hdl.handle.net/11343/359682

Molecular Biology and Evolution, 2025, **42**, 1–14
https://doi.org/10.1093/molbev/msae270
Advance access publication 15 January 2025
Discoveries

MBE OXFORD

Rapid Parallel Adaptation in Distinct Invasions of *Ambrosia Artemisiifolia* Is Driven by Large-Effect Structural Variants

Paul Battlay [1,*] Samuel Craig [1] Andhika R. Putra [2] Keyne Monro [1] Nissanka P. De Silva [1] Jonathan Wilson [1] Vanessa C. Bieker [3] Saila Kabir [1] Nawar Shamaya [1] Lotte van Boheemen [1] Loren H. Rieseberg [4] John R. Stinchcombe [5] Alexandre Fournier-Level [2] Michael D. Martin [3] Kathryn A. Hodgins [1]

[1]School of Biological Sciences, Monash University, Clayton, Victoria 3800, Australia
[2]School of BioSciences, The University of Melbourne, Parkville, Victoria 3010, Australia
[3]Department of Natural History, NTNU University Museum, Norwegian University of Science and Technology (NTNU), Trondheim, Norway
[4]Department of Botany and Biodiversity Research Centre, University of British Columbia, Vancouver, Canada
[5]Department of Ecology and Evolutionary Biology, University of Toronto, Toronto, Ontario M5S3B2, Canada

***Corresponding author:** E-mail: pbattlay@gmail.com.
Associate editor: Michael Purugganan

Abstract

When introduced to multiple distinct ranges, invasive species provide a compelling natural experiment for understanding the repeatability of adaptation. *Ambrosia artemisiifolia* is an invasive, noxious weed, and chief cause of hay fever. Leveraging over 400 whole-genome sequences spanning the native-range in North America and 2 invasions in Europe and Australia, we inferred demographically distinct invasion histories on each continent. Despite substantial differences in genetic source and effective population size changes during introduction, scans of both local climate adaptation and divergence from the native-range revealed genomic signatures of parallel adaptation between invasions. Disproportionately represented among these parallel signatures are 37 large haploblocks—indicators of structural variation—that cover almost 20% of the genome and exist as standing genetic variation in the native-range. Many of these haploblocks are associated with traits important for adaptation to local climate, like size and the timing of flowering, and have rapidly reformed native-range clines in invaded ranges. Others show extreme frequency divergence between ranges, consistent with a response to divergent selection on different continents. Our results demonstrate the key role of large-effect standing variants in rapid adaptation during range expansion, a pattern that is robust to diverse invasion histories.

Keywords: common ragweed, invasion genomics, rapid adaptation, parallel adaptation, local adaptation, inversions, structural variation

Introduction

Invasive species are one of the key drivers of ecological change globally (Pejchar and Mooney 2010; Arneth et al. 2019), posing a significant and growing threat to global biodiversity, agriculture, and human health. They are a leading cause of species extinction worldwide (Clavero and García-Berthou 2005; Pimentel et al. 2005), and the global cost of invasive species—predominantly agricultural yield loss and control measures—was estimated to exceed 423 billion US dollars for 2019 alone (Fokam et al. 2023). Human intervention has so far been insufficient to control the proliferation of biological invasions (Seebens et al. 2017), which are predicted to accelerate as climate change-associated impacts increase (Dukes and Mooney 1999), pointing to the need for a greater understanding of the mechanisms governing invasion success. Here, we use population genomics to determine the genetic mechanisms underlying invasion success in a prolifically invasive weed.

A long-standing mystery in invasion biology is how invasive species can be so successful despite founder effects and bottlenecks that are expected during initial colonization (i.e. the genetic paradox of invasion; Allendorf and Lundquist 2003; Estoup et al. 2016; Schrieber and Lachmuth 2017). Such demographic changes should reduce genetic variation (Willi et al. 2006), cause inbreeding (Angeloni et al. 2011; Fauvergue et al. 2012), and increase the frequency of deleterious alleles (Willi et al. 2013), resulting in depressed fitness and limited adaptive potential. This paradox may be resolved in some cases by repeated introductions, which can lead to high levels of genetic variation in introduced populations thereby mitigating these expected fitness costs associated with colonization (Dlugosch and Parker 2008a; Dlugosch et al. 2015; McGoey and Stinchcombe 2021; Bieker et al. 2022). However, few studies have leveraged invasions with contrasting demographic histories within a single species to assess its influence on the evolutionary trajectories of populations.

When introduced to multiple distinct ranges, invasive species provide a compelling natural experiment for understanding the repeatability in the genetic basis of adaptation. In contrast to the infinitesimal architecture theorized to underlie most adaptive traits (Fisher 1919, 1930), mutations with larger effects on traits are more likely to contribute to adaptation under certain circumstances. For example, when there has been a sudden, large shift

Received: September 24, 2024. **Revised:** November 21, 2024. **Accepted:** December 17, 2024

in adaptive optima (Orr 1998), when populations are small (Charlesworth 2009) or declining (McDonough and Connallon 2023), or if selective pressures vary across space resulting in local adaptation (Yeaman and Whitlock 2011). Large-effect genetic architectures are more likely to result in repeated use of the same gene for adaptation (Yeaman et al. 2018), particularly when adaptation occurs from standing variation (Ralph and Coop 2015), and when there is gene flow between locally adapted populations (Battlay, Yeaman et al. 2024). However, few empirical studies have compared the relative contributions of large- and small-effect variation to parallel adaptation (but see Campbell et al. 2021; Koch et al. 2022). During bottlenecks, beneficial large-effect alleles are more likely to be fixed than those with smaller effects as a result of genetic drift (Charlesworth 2009), but traits controlled by few large-effect loci can have their variance reduced and means shifted (Dlugosch et al. 2015). Consistent with theoretical predictions, large structural variants are increasingly being identified as drivers of rapid adaptation in invasive species (Tepolt and Palumbi 2020; Santangelo et al. 2022; Battlay et al. 2023; Battlay, Hendrickson et al. 2024; Ma et al. 2024; Wilson et al. in press). However, there have been only limited empirical studies of parallelism between invasions at the genomic level (but see van Boheemen and Hodgins 2020; Olazcuaga et al. 2020; Battlay, Hendrickson et al. 2024). Moreover, different invasions may be subjected to population bottlenecks of varying severity, and sourced from distinct genetic clusters in the native-range or other invaded ranges, both of which would reduce the potential for genomic parallelism. It is unclear to what extent such demographic factors influence parallelism, and hence the predictability, of rapid adaptation.

Ambrosia artemisiifolia is a noxious weed, and its airborne pollen is a chief cause of hay fever (allergic rhinitis; Della Torre et al. 1996; Caillaud et al. 2014). As a result of human introductions over the last 200 years, this North American native has successfully colonized all continents except Antarctica. Its recent, aggressive expansion across the globe makes the species a powerful model for understanding parallel rapid adaptation. The presence of latitudinal clines in traits in invading *A. artemisiifolia* populations suggests the involvement of rapid adaptation in the species' spread (Li et al. 2015; van Boheemen, Atwater et al. 2019; McGoey et al. 2020). Furthermore, genomic analyses have implicated the role of large-effect variants in *A. artemisiifolia*'s range expansion (Hämälä et al. 2020; Battlay et al. 2023). Here, we sequenced 95 whole-genomes spanning *A. artemisiifolia*'s invaded Australian range. When combined with 348 whole-genome sequences of contemporary samples from North America and Europe (Bieker et al. 2022), we were able to characterize the invasion history and contrast adaptive change during invasions on two continents. We reconstructed genetically and demographically distinct invasion histories in each introduced range with evidence of a substantial bottleneck in Australia but not in Europe. These data provide a case study of whether genetic bottlenecks limit the extent of parallel adaptive evolution from standing variation. By comparing the extent of parallel signatures of adaptation between the introduced ranges, we discovered that genomic repeatability was high regardless of the invasion history. This repeatability occurred disproportionately in large structural variants that cover ~20% of the genome and underpin substantial variation in locally adaptive traits such as flowering time. These results underscore the importance of standing variation in large-effect structural variants in rapid, repeated adaptation during range expansions with distinct demographic histories.

Results

Contrasting Invasion Histories in Europe and Australia

A principal component analysis (PCA) of genetic variation across 443 whole genome-sequenced *A. artemisiifolia* samples (Fig. 1a; supplementary table S1, Supplementary Material online) revealed little evidence of divergence between North America and Europe, consistent with previous inferences of repeated introductions from North America (van Boheemen et al. 2017; Bieker et al. 2022; Fig. 1b). Most European samples overlapped with North American mid-east and west clusters, with no evidence that the North American south cluster (which comprises samples from Florida) contributed to European introductions (Fig. 1b). In contrast to the genetic similarity between North American and European samples, there is substantial divergence between the main genetic cluster of Australian samples and samples from the other ranges. The main Australian cluster shows the highest similarity with the North American south and mid-east clusters (Fig. 1b), but Australian samples outside this main cluster group more closely with North American east samples (Fig. 1b) and are largely found in the southernmost Australian population (Nelligen, NSW; supplementary fig. S1, Supplementary Material online). Admixture proportions measured across samples support these observations (supplementary fig. S2, Supplementary Material online). These results suggest European and Australian invading populations were founded by distinct sources within the native-range.

To determine the most likely scenarios of divergence and admixture in the four native-range genetic-spatial clusters (Bieker et al. 2022) and the two invaded ranges, we used *DIYABC-RF* (Collin et al. 2021). The best-supported scenario for the development of genetic structure in the native-range modeled the division of a common ancestral population into south and west clusters, with the independent admixture of these clusters resulting in the formation of the mid-east and east clusters (posterior probability $P = 0.534$; supplementary fig. S3 and table S2, Supplementary Material online). The best-supported scenario for the European invasion modeled a primary introduction from the west cluster followed by an independent secondary introduction from the mid-east cluster, whereas the best-supported Australian scenario modeled introductions from the mid-east cluster and south cluster with ambiguity regarding order of arrival (posterior probability $P = 0.473$; Fig. 1c; supplementary fig. S4 and tables S3 and S14, Supplementary Material online).

To further identify the invasion sources, we trained a deep neural network on genetic variation from the North American range using *Locator* (Battey et al. 2020), and predicted source locations for samples from each invaded range. *Locator* results were consistent with those from PCA and *DIYABC-RF*, with most European samples showing northern North American ancestry and most Australian samples showing ancestry from further south (Fig. 1d). The Australian samples that grouped separately from the main Australian cluster on the PCA were predicted to have been sourced from much further to the north and east of North America (supplementary fig. S1, Supplementary Material online), consistent with their location on the PCA. Comparisons of climatic data for introductions and their

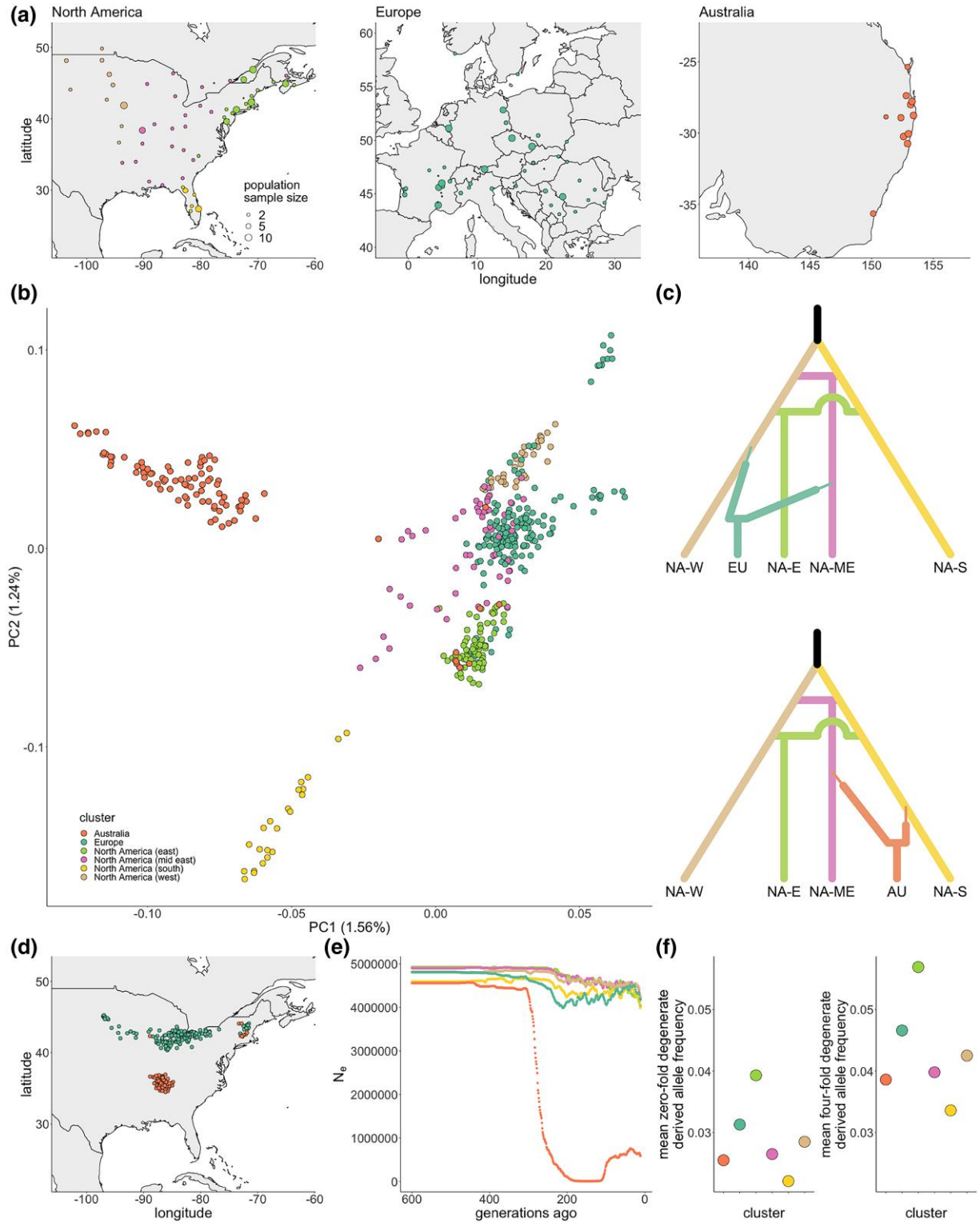

Fig. 1. Invasion sources and recent demography of *A. artemisiifolia*. a) Sampling locations for 443 *A. artemisiifolia* whole-genome sequences spanning 119 populations across 3 ranges. b) Mapping of individual samples along the first 2 principal components of 100,000 LD-thinned genetic variants sampled from outside genes and haploblocks, colored by North American cluster or invaded range. c) The most likely scenarios from DIY-ABC modeling historic divergence between native-range genetic clusters (NA-W: North America west; NA-ME: North America mid-east; NA-S: North America south; NA-E: North America east) and introductions to Europe (EU) and Australia (AU). Time is not to scale. d) Deep neural network-predicted source locations in North America for invasive European and Australian samples. e) Effective population sizes (N_e) over time inferred from LD in each North American cluster or invaded range. f) Mean allele frequency at zero-fold and 4-fold degenerate sites for invaded ranges and North American clusters. Based on 95% CIs from bootstrapping sites, all points are significantly different from one another. CIs are too narrow to show on the plot.

putative sources revealed patterns consistent with preadaptation. Climate niches inhabited by Australian and European populations roughly correspond to the putative sources of each invasion in North America (supplementary fig. S5, Supplementary Material online) and this is reiterated by the strong relationship between absolute population latitude and

Locator source location prediction (supplementary fig. S5, Supplementary Material online).

Linkage disequilibrium (LD)-based approaches provide the best estimates of effective population size following recent demographic shifts (Nadachowska-Brzyska et al. 2022). We used one such method, *GONE* (Novo et al. 2023) in each North American cluster and each invaded range, and found evidence of a recent population bottleneck in Australia (a 416-fold reduction in effective population size) but not in North America or Europe (Fig. 1e). We also measured the average frequency of derived zero-fold degenerate alleles—a metric designed to estimate genetic load (Simons and Sella 2016)—in North American clusters and each invaded range. Load estimates in each invaded range reflected their North American cluster ancestry rather than demographic events during invasion (Fig. 1f). Furthermore, similar patterns were observed in putatively neutral 4-fold degenerate sites (Fig. 1f). Together these results suggest the invasions of Europe and Australia were distinct both in terms of genetic sources and demographies.

Large Structural Variants Support Adaptive Trait Evolution

By analyzing local genomic population structure across all 443 samples in our dataset, we identified and genotyped 37 haploblocks (population-genomic signatures of large structural variants; supplementary table S4, Supplementary Material online), including the 15 previously described in (Battlay et al. 2023). Haploblocks ranged in size from 0.7 to 17.3 Mbp, cumulatively covered 18.5% of the genome, and varied in frequency between ranges (Fig. 2a). Fifteen of the 37 haploblocks (40%) corresponded to structural variants that were heterozygous in our diploid reference assembly (supplementary fig. S6 and table S4, Supplementary Material online). While all haploblocks that are heterozygous in the reference include inversions, some are more complex (e.g. *hb-chr9* includes a large deletion in the inverted haplotype, while *hb-chr8* consists of three tandem inverted regions that appear to segregate as a single structural variant; supplementary fig. S6, Supplementary Material online).

To assess the involvement of haploblocks in adaptation to local climate, we compared the change in allele frequency in response to absolute latitude for haploblocks and 10,000 randomly sampled SNPs located outside haploblocks and genes. Absolute latitude was used as a proxy for climate in this analysis as it is highly correlated with the first principal component of climate variation across sampling locations in this study ($r^2 = 0.47$; supplementary fig. S5, Supplementary Material online). The majority of haploblocks showed evidence of local climate adaptation: of the 37 haploblocks, 30 (81%) were significant (i.e. had slopes in the 5% tail of the slope distribution) in at least one range, and North America, Europe, and Australia had 21 (57%), 10 (27%), and 18 (47%) significant haploblocks, respectively (Fig. 2b; supplementary table S5, Supplementary Material online). Nine haploblocks showed evidence of parallel climate adaptation between North America and at least one invaded range, with slopes significant and in the same direction in each range (Fig. 2c; supplementary table S5, Supplementary Material online). For one haploblock, *hb-chr5b*, significant slopes were observed in parallel across all three ranges (Fig. 2c; supplementary table S5, Supplementary Material online).

To understand the contributions of haploblocks to locally adaptive traits such as size and the timing of flowering, we performed genome-wide association studies (GWAS) using 226 samples from across the three ranges with common-garden phenotypes previously measured by van Boheemen, Atwater, and Hodgins (van Boheemen, Atwater et al. 2019). Ten haploblocks harbored an enrichment of windows (hypergeometric P-value < 0.05 Bonferroni-corrected for multiple tests across haploblocks) that were associated (0.1% tail of the genome-wide distribution) with at least one of the 13 phenotypes (supplementary table S6, Supplementary Material online). Several haploblocks were associated with multiple traits (e.g. *hb-chr2*; Fig. 2d), and flowering-time phenotypes showed associations with the greatest number of haploblocks (Fig. 2d). All haploblocks associated with flowering-time phenotypes contained *Arabidopsis thaliana* flowering-time gene orthologs (Bouché et al. 2016; supplementary table S7, Supplementary Material online), but this only constituted a significant enrichment for the 16 orthologs in *hb-chr5b* (Fisher's exact test P-value = 0.001; supplementary table S7, Supplementary Material online) which also colocalizes with a large-effect flowering-time QTL in *A. artemisiifolia* (Prapas et al. 2022). Correspondingly, genes across all haploblock regions were enriched for gene ontology (GO) terms related to phenology (e.g. floral organ senescence; regulation of flower development) as well as defense (e.g. regulation of innate immune response; regulation of defense response; supplementary table S8, Supplementary Material online), which are important traits for local adaptation in this species (van Boheemen, Atwater et al. 2019; van Boheemen, Bou-Assi et al. 2019). To understand the contribution of haploblocks to GWAS phenotypes, we partitioned for each trait the variance explained by associated haploblocks from the rest of the genomic background represented by a genetic relatedness matrix. Models for 10 traits showed support for background additive genetic variance. For eight of these 10 traits, a significant proportion of the variance was attributable to genetic effects located in haploblocks, which explained between 14.4% and 63.6% of trait variation (supplementary table S9, Supplementary Material online; Fig. 2e).

Genomic Signatures of Selection Reveal the Extent of Parallel Evolution

Matching climate associations between native and invaded ranges suggest rapid parallel adaptation has occurred in the invaded ranges to re-establish patterns of local adaptation to climate present in the native-range. To address this quantitatively, we first looked for extreme allele frequency divergence between populations within each range as a measure of local adaptation (XtX; Gautier 2015). We also measured the rank correlation τ (Kendall 1938) between allele frequency in each range and four independent bioclimatic variables (BIO1: annual mean temperature; BIO2: mean diurnal range; BIO12: annual precipitation; BIO15: precipitation seasonality). For each variable in each range, the 5% tail of the XtX outlier window distribution was significantly enriched for windows in the 5% tail of correlations with each climate variable ($P \leq 2.5 \times 10^{-23}$; supplementary table S10, Supplementary Material online). This suggests that local climate adaptation is a strong driver of allele frequency divergence in each range. Overall, 77.5%, 28.4%, and 43.8% of North American, European, and Australian XtX outlier windows, respectively were also correlated with at least one environmental variable, which is consistent with adaptive differentiation in response to climate. These "XtX-EAA" climate adaptation candidate windows

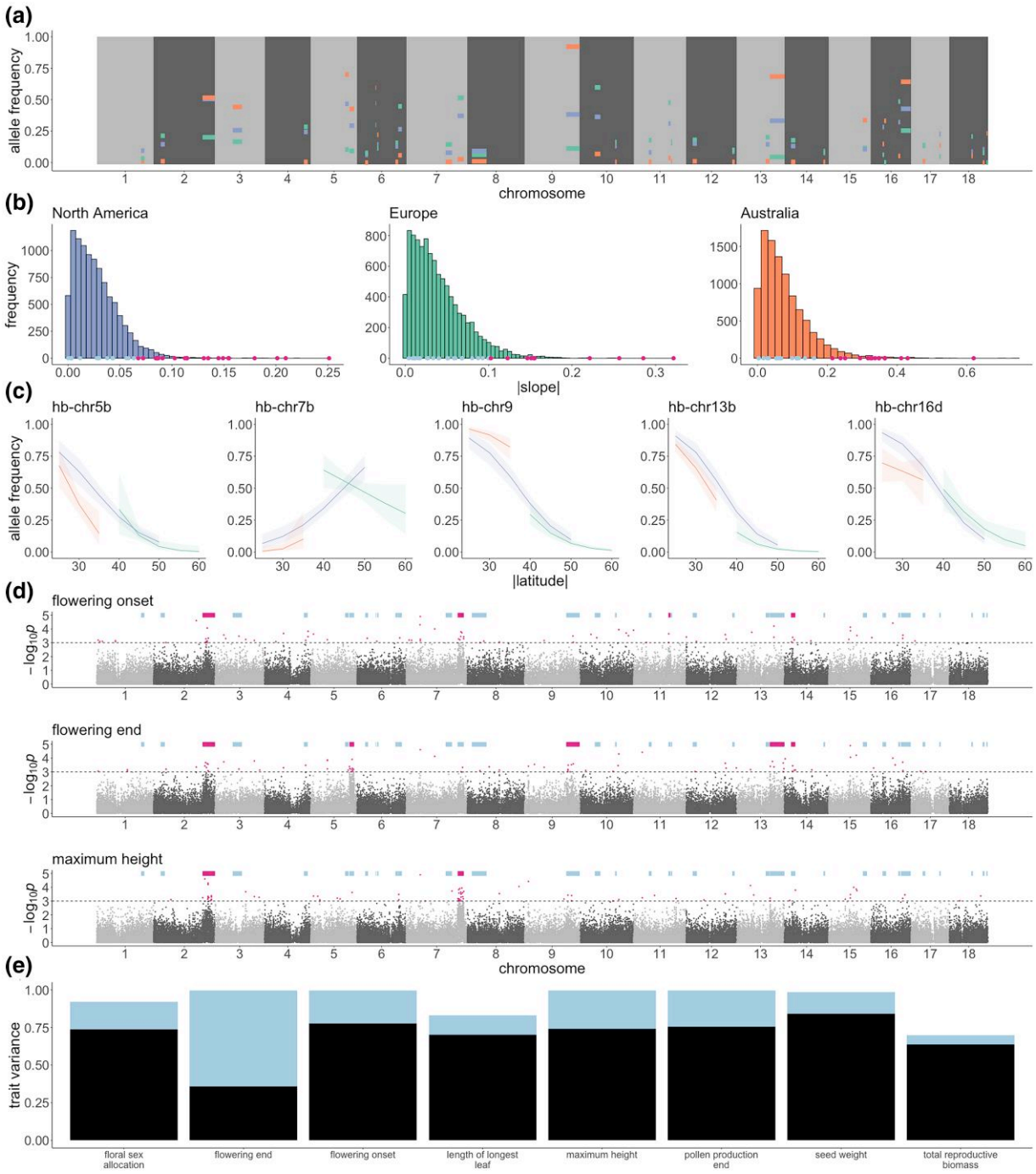

Fig. 2. Geographic distributions and phenotypic associations for haploblocks across three ranges (North America: blue; Europe: green; Australia: orange). a) Genomic location and frequency of each haploblock in each range. b) Distributions of slope estimates of allele frequency as a function of latitude in each range for 10,000 random SNPs (histograms) with slope estimates for haploblocks indicated below in blue, or pink for those haploblocks in the 5% tail of the slope distribution. c) Logistic regression models with error bands representing 95% CI of least-squares regressions of haploblock frequency against latitude. d) Manhattan plots (log-transformed empirical *P*-values for 10 kbp analysis window scores against genomic location) for three phenotypes. Pale blue bars indicate the location of haploblocks. Pink bars denote haploblocks that are enriched for the windows in the 0.1% tail of the *P*-value distribution (indicated by pink points and the dotted line). e) Variance explained by different types of genetic variation for the eight traits that showed significant contributions of GWAS outlier-enriched haploblocks (blue) and polygenic background (black).

showed significant parallelism between ranges in each pairwise comparison ($P \leq 1.37 \times 10^{-66}$; Fig. 3a; supplementary table S10, Supplementary Material online) and were enriched in 19, six, and four haploblock regions in North America, Europe, and Australia, respectively (supplementary fig. S7 and table S11, Supplementary Material online). The greater number of XtX-EAA windows and climate-associated haploblocks in North America when compared to the invaded ranges is consistent with long-established local adaptation in the native-range and incomplete, ongoing adaptation to climate on continents where *A. artemisiifolia* has recently been introduced.

Dramatic shifts in allele frequencies between invasive and native-ranges are strong indications of rapid adaptation following introduction. To identify regions of the genome showing

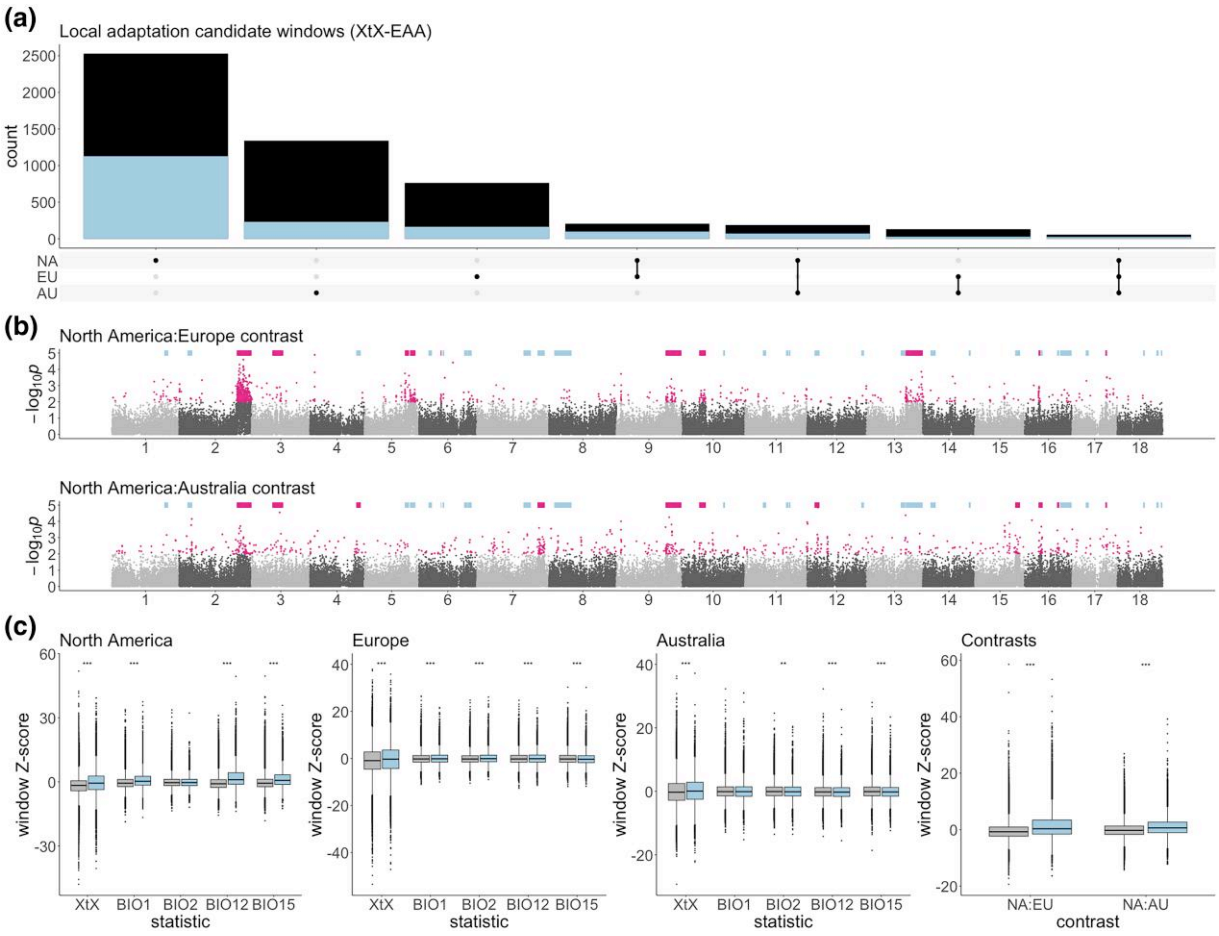

Fig. 3. Genomic signatures of parallel rapid adaptation. a) Upset plot showing counts of and overlaps between XtX-EAA local adaptation candidate windows in each range (black columns), all of which are enriched for the presence of windows within haploblock regions (blue columns). b) Manhattan plots (log-transformed empirical *P*-values for 10 kbp analysis window scores against genomic location) for contrast scans between North America and each invaded range. Pale blue bars indicate the location of haploblocks. Pink bars denote haploblocks that are enriched for the windows in the 1% tail of the *P*-value distribution (indicated by pink points). c) *Z*-score distributions of 10 kbp windows for genome scans in haploblock (blue) and nonhaploblock (gray) regions of the genome. Asterisks represent *P*-values from Mann–Whitney *U* tests comparing means between haploblock and nonhaploblock regions (*: $P < 0.05$; **: $P < 0.01$; ***: $P < 0.001$).

such signatures of selection, we computed the BayPass contrast statistic (Olazcuaga et al. 2020) to compare allele frequencies across each invaded range with their likely source in the native North American range separately. We supplemented contrast analyses with selective sweep scans in individual ranges using Fay and Wu's *H* (Fay and Wu 2000). Genomic windows showing evidence of native-invasive divergence (contrast outlier windows) showed far more overlap with invasive-range sweep outlier windows (extreme negative *H* values) than those from North America, consistent with rapid adaptation occurring in each introduced range during invasion (3 vs. 96 and 4 vs. 43 for North America:Europe and North America:Australia contrasts respectively; supplementary fig. S8, Supplementary Material online). Among the 1% tail of native-invasive divergence there was significant parallelism between ranges ($P = 1.44 \times 10^{-76}$; supplementary table S10, Supplementary Material online). Ten and 12 haploblocks were enriched for contrast outliers in Europe and Australia contrasts respectively, with six (*hb-chr2b*, *hb-chr3*, *hb-chr9*, *hb-chr10a*, *hb-chr16a*, and *hb-chr17b*) showing enrichment in both ranges (Fig. 3b; supplementary table S11, Supplementary Material online).

To determine whether regions of the genome harboring large structural variants are more likely to contain candidates for adaptation, we asked whether genomic windows in haploblock regions contained significantly more extreme values on average (i.e. more evidence for a role in adaptation) than windows in non-haploblock regions of the genome. For all within-range XtX, most correlations with environmental variables, and both native:invaded range contrasts, genome-wide signatures for adaptation were significantly higher in haploblock regions (Fig. 3c; supplementary table S12, Supplementary Material online).

Discussion

Leveraging whole-genome resequencing of *A. artemisiifolia* samples spanning the native North American range and two introduced ranges in Europe and Australia, we reconstructed the demographic history of these two invasions. Europe was colonized through multiple introductions from across North America, but ancestry from the North American south cluster (Florida) appears absent. Contrastingly, Florida appears to be a major source of genetic variation in Australian populations (along with the mid-east cluster; Fig. 1b–d). It is often observed that a species' native and invasive populations occupy similar climate niches (Liu et al. 2020), and the climatic conditions in native

environments of *A. artemisiifolia* broadly correspond to those in the invasive ones that they seeded (supplementary fig. S5, Supplementary Material online). Climate matching like this suggests that preadaptation has played a role in determining the success of this invader, and is consistent with predictions from genetically informed species distribution modeling in this species (Putra et al. 2023). However, preadaptation does not preclude the occurrence of post-introduction adaptation (Sherpa and Després 2021). The results of this study provide compelling empirical evidence of repeated rapid adaptation in *A. artemisiifolia* invasions facilitated by large-effect structural variants introduced from the native-range.

Substantial differences exist between the European and Australian invasions of *A. artemisiifolia*. European *A. artemisiifolia* occupies diverse climatic conditions and has been present on the continent for over 200 years (Chauvel et al. 2006), while Australian *A. artemisiifolia* occupies a more restricted range of climates (van Boheemen, Atwater et al. 2019; Putra et al. 2023) and was first recorded in Australia in 1908 (Parsons and Cuthbertson 2001). The results of our demographic analyses highlight further differences between the invasions of Europe and Australia. Notably, the importance of different sources from within the native-range to each invasion (Fig. 1c), and the evidence of a strong bottleneck in the Australian, but not the European invasion (Fig. 1e). European results are consistent with previous analyses which suggest that multiple introductions to Europe have prevented or ameliorated the occurrence of a bottleneck during this invasion (van Boheemen et al. 2017; Bieker et al. 2022). Results of a previous analysis of the Australian invasion (van Boheemen et al. 2017) are consistent with our inference of a bottleneck during introduction. In contrast with our results, van Boheemen et al. (2017) inferred the source of the Australian invasion to be within the European range. However, they did not extensively sample Florida, a major contributor to the Australian invasion in our analysis, which underscores the importance of exhaustive sampling of native-range in demographic studies of invaders.

Invasion events have long been theorized to be associated with population bottlenecks (Baker and Stebbins 1965), resulting in decreased effective population sizes and reductions in genetic variation (Nei et al. 1975). However, studies have emphasized the role of multiple introductions in buffering invasions from bottlenecks (Dlugosch and Parker 2008a; van Boheemen et al. 2017), while meta-analyses of empirical data suggest that loss of genetic diversity does not limit the success of invasive species (Uller and Leimu 2011; He et al. 2024). Furthermore, reduced genetic diversity does not necessarily limit adaptive evolution (Dlugosch and Parker 2008b; Estoup et al. 2016), nor does it need to be overcome by de novo mutations (Dogantzis et al. 2024). Bottlenecks may also affect the abundance of deleterious alleles, which can increase due to genetic drift (Whitlock and Davis 2011), or be purged due to inbreeding (Marchini et al. 2016). Importantly, the drop in Australian effective population size does not appear to have resulted in the accumulation of deleterious alleles (estimated from the average derived allele frequency across zero-fold degenerate sites). These values are similarly low in Australia and the invasion's North American sources (Fig. 1f), suggesting that the bottleneck has not been long or severe enough to cause an increase in genetic load, despite causing reductions in genetic diversity (van Boheemen et al. 2017; Fig. 1e).

Invasive species introduced to multiple ranges provide a natural experiment to assess the repeatability of adaptation during range expansion (Bock et al. 2015). Repeated genetic evolution reveals constraints and biases in the genetic routes to adaptive optima (Conte et al. 2012; Yeaman et al. 2018), and hence the predictability of adaptation. Furthermore, repeatability suggests the involvement of genetic architectures featuring genetic variants of large effect (Chevin et al. 2010). Population-genomic analyses of parallel invasions are beginning to provide important empirical support in these areas. Repeatability between invaded ranges has been observed in diverse taxa (van Boheemen and Hodgins 2020; Olazcuaga et al. 2020; Battlay, Hendrickson et al. 2024), in some cases involving large-effect variants (Battlay, Hendrickson et al. 2024). Our findings, that the invasion histories of *A. artemisiifolia* in Europe and Australia are distinct, allow us to examine the extent to which demography affects these patterns. We have previously described genomic signatures of local climate adaptation in parallel between the native North American range and the invasive European range (Battlay et al. 2023). Here, we demonstrate that similar signatures of repeatability are found in the invasion of Australia, and moreover exist between invasions of Europe and Australia. We also observe genomic signatures of adaptive divergence from the native-range in parallel between Europe and Australia, reflecting shared genetic changes across multiple independent invasions.

Across our 443 samples we have identified 37 large haploblocks that cover almost 20% of the genome and show features consistent with chromosomal inversions—15 of these haploblocks correspond to inversion polymorphisms segregating in our diploid reference genome assembly (supplementary fig. S6, Supplementary Material online). By leveraging common-garden data from samples spanning all three ranges, we observe that many haploblocks are associated with traits that are important for local climate adaptation (Fig. 2d) and that haploblocks explain a substantial proportion of the variance in these traits (Fig. 2e). Correspondingly, regions harboring haploblocks are enriched for genomic signatures of local adaptation (Fig. 3c). Inversions are predicted to play an important role in local adaptation by maintaining complementary combinations of alleles in blocks of reduced recombination (Kirkpatrick and Barton 2006; Kirkpatrick and Barrett 2015). However, when populations encounter novel environments, inversions may inhibit adaptation by restricting optimal combinations of alleles (Roesti et al. 2022). And while large-effect standing variants are more likely to be involved in parallel adaptation (Ralph and Coop 2015; Yeaman et al. 2018), whether and under what conditions this would apply to inversions is less clear (Westram et al. 2022). Nevertheless, haploblocks appear to play a key role in parallel adaptation in this species. In many cases, haploblock allele frequency clines present in the native-range have rapidly reformed in invaded ranges (Fig. 2b and c). Haploblocks are also disproportionately represented in parallel divergence between native and invaded ranges. Of the 98 outlier windows shared between North America:Europe and North America:Australia contrasts, 70 occur in haploblocks ($P = 7.79 \times 10^{-20}$). The haploblocks of *A. artemisiifolia* are predominantly (if not completely) standing variation in the native-range, where we observe in our data segregation of 36 of the 37 haploblocks (Fig. 2a). Despite the disproportionately large role played by haploblocks in parallel adaptation, the majority of parallel windows occur outside of haploblocks (Fig. 2a). This suggests that variants of more modest effect can still contribute to parallel adaptation (e.g. Koch et al. 2022).

As the number of biological invasions worldwide continues to grow, understanding the extent, genetic architecture and predictability of range expansion in invasive species becomes ever more salient. Our results showcase the remarkable parallel adaptation that has occurred as demographically distinct introductions of *A. artemisiifolia* have invaded Europe and Australia over the last 200 years. Central to this result are 37 large structural variants, which underscore the role of large-effect standing variation in rapid and repeated adaptation during invasion. The observed strong signatures of selection on these variants in Australia add to mounting empirical evidence that bottlenecks do not necessarily limit adaptation.

Methods

A. Artemisiifolia Samples

We generated whole-genome resequencing data for 95 specimens of *A. artemisiifolia* collected from the east coast of Australia in 2014 and described in (van Boheemen, Atwater et al. 2019). We combined this data with whole-genome resequencing of 348 *A. artemisiifolia* specimens collected from North America ($n = 179$) and Europe ($n = 169$) between 2007 and 2019 and previously described in (Bieker et al. 2022). See supplementary table S1, Supplementary Material online for details of each sample.

Whole-genome Resequencing

Illumina libraries were prepared following the approach of (Bieker et al. 2022). Leaf tissue was collected and stored in silica gel desiccants (Chase and Hills 1991) at room temperature until required for DNA extraction. Approximately 20 to 30 mg of dried leaf tissue from each sample were placed inside a 2.0-ml tube with a 3-mm stainless steel bead and ground with a TissueLyser II (QIAGEN). The DNA was extracted using a modified CTAB protocol (Doyle and Doyle 1987) adapted for a 96-well plate format (Ivanova et al. 2008) using EconoSpin filter plates, and the DNA was suspended in 60 µl of elution buffer. Extracted DNA was quantified using a Qubit 2.0 fluorometer (Invitrogen, Carlsbad, CA, USA) using dsDNA Quantitation HS (high sensitivity, 0.2 to 120 ng) kit. Extraction blanks were prepared alongside the samples to monitor possible contamination. Extracts were converted into blunt-end Illumina libraries as described above using BEST protocol (Carøe et al. 2018), in which custom blunt-end adapters (Meyer and Kircher 2010) were ligated to the DNA fragments. Dual-index libraries were generated using custom index primers during indexing PCR. Indexing PCR was carried out in a 50-µl reaction using 10 µl of library template, 0.2 µM sample-specific forward index primer, 0.2 µM sample-specific reverse index primer, 1× Platinum SuperFi PCR master mix, and the rest of the volume filled up with molecular-grade water. The PCR was performed with an initial denaturation of 3 min at 95 °C, followed by 12 cycles of a 20-s denaturation at 98 °C, 60 s of annealing at 60 °C, and 60 s of extension at 72 °C, followed by a final extension for 5 min at 72 °C. Amplified libraries were purified with SPRI beads (Rohland and Reich 2012) and eluted in 33 µl of EBT buffer. The samples were sent to GENEWIZ (Suzhou, China) and sequenced on one lane of Illumina NovaSeq 6000 PE150, which yielded 935 Gbp of data.

Alignment and Variant Calling

Each pair of FASTQ files from 95 Australian *A. artemisiifolia* samples were aligned to the primary haplotype of the phased, diploid reference assembly described in (Battlay et al. 2023) using the *Paleomix* pipeline v.1.2.13.4 (Schubert et al. 2014), which incorporates *AdapterRemoval* v.2.3.1 (Schubert et al. 2016), *BWA* v.0.7.17 (Li 2013), *Picard* v.2.19.0 *MarkDuplicates* (https://broadinstitute.github.io/picard/), and GATK v.3.7 *IndelRealigner* (Van der Auwera and O'Connor 2020). For *AdapterRemoval*, we trimmed undefined bases (–trimns: yes), trimmed low-quality bases from the ends of reads (–trimqualities: yes), and collapsed overlapping reads (–collapse: yes). The maximum number of mismatches for adapter matching was 3 (–mm 3) and the minimum length of reads to be retained was 25 bp (-minlength 25). For BWA, we used the mem algorithm with default parameters. Mean depths of alignments ranged from 1.2× to 15.6× with a mean of 5× (supplementary table S1, Supplementary Material online). Variants were called across the resulting 95 BAM files from Australian samples and 348 BAM files previously generated from North American and European samples (Bieker et al. 2022; Battlay et al. 2023). GATK v.3.8 *UnifiedGenotyper* (DePristo et al. 2011) was used to call variants on all contigs >100 kbp in length. GATK v.3.8 *VariantFiltration* (Van der Auwera and O'Connor 2020) and *VcfTools* v.0.1.16 (Danecek et al. 2011) were used to filter variant calls. SNP and indel calls were separately filtered using GATK hard-filtering recommendations (SNPs: QD < 2.0, FS > 60.0, SOR > 3.0, MQ < 40.0, ReadPosRankSum < −8.0, MQRankSum < −12.5; indels: QD < 2.0, FS > 200.0, SOR > 10.0, ReadPosRankSum < −20.0, InbreedingCoeff < −0.8). In addition, SNPs and indels were separately filtered for sites with depth (DP) <1 SD below the mean, and >1.5 SDs above the mean. Individual genotypes were set to missing if their depth was <3, then variants with >20% missingness across all samples were removed. Samples with >60% missing variants were removed. For the remaining 397 samples, genotypes were phased and imputed using Beagle v.5.4 (Browning et al. 2018).

Population Structure

To calculate genotype likelihoods, we ran *angsd* v0.939 (Korneliussen et al. 2014) on alignments of 443 samples, including only sites that could be estimated in >75% of samples (-minInd 333). We used the GATK genotype likelihood model (-GL 2), inferred the major and minor alleles from the data (-doMajorMinor 1), inferred minor allele frequencies using genotype likelihoods (-doMaf 2), and disabled genotype calling (-doGeno −1). We retained reads with a minimum mapping quality of 30 (-minMapQ 30), retained bases with a minimum quality score of 20 (-minQ 20), and retained sites with a SNP P-value $< 1 \times 10^{-6}$ (-SNP_pval 1e-6) and which were supported by a minimum of 2 uniquely mapping reads per individual (-uniqueOnly 1 -setMinDepthInd 2). We filtered out sites with a minor allele frequency <0.05 (-minMaf 0.05), counted bases at each position (-doCounts 1), and produced beagle(-doGLF 2) and plink (-doPlink 2) output files. A list of LD-pruned variants was generated in *plink* v1.9 (Chang et al. 2015) using a window size of 50 kbp, a step size of 5 SNPs, and an r^2 threshold of 0.5 (–indep-pairwise 50 5 0.5). Sites were filtered to include only those that were LD-pruned and also outside annotated genes and haploblocks, and then randomly downsampled to 100,000. A covariance matrix was generated from these filtered sites using *pcangsd* v.1.2

(Meisner and Albrechtsen 2018) and used for PCA in R v.4.3.1. Admixture analysis was performed using *NGSadmix* v.0.939 (Skotte et al. 2013) and the same genotype likelihoods as the PCA. We ran analyses for two to six ancestral populations (K). Ten independent runs with different seeds were performed for each K value. The run with the highest likelihood for each K was used for plotting (supplementary fig. S2, Supplementary Material online).

Demographic Modeling

We implemented an approximate Bayesian computation (ABC) random forest (RF) statistical framework using *DIYABC-RF* (Collin et al. 2021) to model the formation of genetic structure in the native-range, infer the introduction source of the invaded ranges, and to estimate demographic parameters of *A. artemisiifolia*. For this ABC-RF analysis, we divided North America into the four clusters previously defined (Bieker et al. 2022) based on *ADMIXTURE* results and geography. We used all samples for which SNPs were called, excepting the southernmost Australian population, which appeared separate to the main genetic cluster (AU01; supplementary fig. S1, Supplementary Material online). SNPs were LD-pruned with *plink* 2.0 alpha (Chang et al. 2015) using a window size of 50 kbp, a step size of 5 SNPs, and an r^2 threshold of 0.2 (indep-pairwise 50 5 0.2) and filtered out minor allele frequencies <0.05. We built on the ABC-RF analysis of (van Boheemen et al. 2017), modeling both the development of genetic structure in the native-range in addition to incorporating independent introduction and bridgehead introduction scenarios for each invaded range (supplementary figs. S3 and S4, Supplementary Material online). For the introduction scenarios, we used the priors defined in (van Boheemen et al. 2017; supplementary table S13, Supplementary Material online), to which readers are directed for detailed description.

To model the formation of genetic structure in the native-range of *A. artemisiifolia*, we simulated datasets from nine branching pattern topologies, each with three temporal parameter configurations, for all permutations of the four sampled native-range populations (supplementary fig. S3, Supplementary Material online). To manage the number of native-range scenarios to be compared with ABC-RF, we opted for a sequential approach to model selection. This approach first compared subsets of scenarios—defined by topology—before comparing the best-supported scenarios between subsets to determine the overall best scenario (supplementary fig. S3 and table S2, Supplementary Material online) (Byrne et al. 2022). In a stepwise manner, we conducted independent analyses of the introduction of *A. artemisiifolia* to Europe and Australia, incorporating the results of the preceding native-range analysis (supplementary fig. S4 and table S3, Supplementary Material online) (Fontaine et al. 2021). In the final analysis, we compared the best-supported scenarios of independent introduction with bridgehead introductions from Europe to Australia (supplementary table S14, Supplementary Material online). Further details of the implementation of this method are provided in the supplementary materials.

Invasion Source Prediction

To predict source locations of invasive *A. artemisiifolia* populations, we used *Locator* (Battey et al. 2020) and SNP data from the 397 samples for which SNPs were called (supplementary table S1, Supplementary Material online). All SNPs with a minor allele frequency <0.05 were included in the analysis. Models were trained using sampling location (latitude; longitude) and genotype data for all samples across the putative source range and then the locations of invasive-range individuals were predicted by the model. For Europe, we used North America as the source range. For Australian samples, we initially included North America and Europe as sources, but as all Australian source locations in this pilot run were predicted to be much closer to North America than Europe, we subsequently used only the North American range as a source for Australian samples. We ran Locator in 10-Mbp nonoverlapping windows across the genome, and averaged each prediction location across these 113 genomic windows.

Effective Population Size

We used *GONE* (Novo et al. 2023) to estimate effective population size in each range over time. In North America and Europe, we used all samples for which SNPs were called ($n = 155$ for each range). In Australia, we only included the 78 samples that were in the main genetic cluster (see Fig. 1b; supplementary table S1, Supplementary Material online) to avoid the confounding effects of population structure on estimates of effective population size (Novo et al. 2023). In each range and for each North American cluster, *GONE* was run using 100,000 SNPs sampled from outside haploblock regions, with the recombination rate parameter was set to 1.428 cM/Mbp based on the genetic map described by Prapas et al. (2022).

Estimation of Genetic Load

To identify zero-fold and 4-fold degenerate sites throughout the genome, we developed a Python script to systematically examine all possible codons (based on the reference annotation (Battlay et al. 2023) for substitutions that always (zero-fold degenerate) or never (4-fold degenerate) result in amino acid substitutions. We analyzed each invaded range and each North American genetic cluster separately. Within each range or cluster, we randomly downsampled the number of individuals to equal the number of individuals in the group with the smallest sample size (North America [south]; $n = 22$) and used *angsd* v.0.939 (Korneliussen et al. 2014) to calculate the frequency of derived sites in each group (-GL 2 -doMaf 2 -minQ 20 -minMapQ 30 -minInd 4), using the consensus of resequencing data from 2 outgroup species (*Ambrosia chamissonis* and *Ambrosia carduacea*; Bieker et al. 2022) mapped to the reference to determine the ancestral state at each site (-doMajorMinor 5 -anc). We calculated the mean frequencies of genome-wide derived zero-fold and 4-fold degenerate mutations for each group and performed bootstrapping by drawing 20% of sites for each group to recalculate means, which was repeated 100 times.

Haploblock Identification

We identified haploblocks (indicative of large structural variants) using local PCA, modifying the method described by Li and Ralph (2019) to utilize covariance matrices from *pcangsd* v.1.2 (Meisner and Albrechtsen 2018), which were calculated in 100-kbp windows from beagle files generated in *angsd* v.0.939 (Korneliussen et al. 2014) (-GL 2 -doMajorMinor 1 -doCounts 1 -doGLF 2 -SNP_pval 1e-6

-doMaf 2 -doGeno −1 -minMapQ 30 -minQ 20 -minMaf 0.05 -setMinDepthInd 2 -uniqueOnly 1 -doPlink 2) on alignments of 443 samples, including only sites that could be estimated in >75% of samples (-minInd 333). Local population structure along each chromosome was analyzed on 5 MDS axes and outliers were identified from the 5% corners of each pair of MDS axes. Candidate haploblocks were identified by manual examination of MDS plots for each chromosome. Across each candidate region local PCAs were performed with *angsd* and *pcangsd* using the same parameters used for the 100 kbp windows. Heterozygosity was also calculated for each sample in each candidate region using *angsd* (-minMapQ 30 -minQ 20 -trim 5 -GL 2), outputting a site allele frequency file from genotype likelihoods (-dosaf 1) for analysis by *realSFS* v.0.939 (Nielsen et al. 2012) with a folded site frequency spectrum (-fold 1). Haploblocks were identified by the presence of 3 clusters of samples along a single principal component axis, indicative of two homozygous and one heterozygous inversion genotype, as well as by the presence of elevated heterozygosity in the region for samples genotyped as heterozygotes. We defined elevated heterozygosity as when the standard error of the mean (SEM) for each homozygote class did not overlap the SEM for the heterozygote class. We validated haploblock genotypes by performing LD scans with *ngsLD* (Fox et al. 2019) v.1.2.0 with no maximum distance for LD calculation (−max_kb_dist 0) on 5,000 randomly sampled sites with minor allele frequencies >0.05 (−min_maf 0.05) from each chromosome containing a haploblock. For each haploblock, LD scans were run on all samples, as well as a set of samples homozygous for the more common haploblock allele. To identify inversions segregating in our diploid reference that corresponded to population-genomic haploblock signatures, we aligned the two haplotypes of our reference (Battlay et al. 2023) using *minimap* v.2.1.8 (Li 2018) with a kmer size of 19 (-k19), a window size value of 19 (-w19), and a mapping quality threshold of 200 (-m200). After filtering out alignments that were shorter than 10 kbp or that contained fewer than 5,000 matches, we visualized *minimap* alignments using the R package *pafr* and manually compared them to MDS manhattan plots of local PCA results (supplementary fig. S6, Supplementary Material online).

Haploblock-latitude Slopes

To identify haploblocks exhibiting clinal patterns, we used generalized linear models to assess how the allele frequency of each haploblock (and 10,000 SNPs sampled from outside haploblocks and genes) changed with latitude in each range separately. We designated significant slopes as those slopes that fell into the 5% tail of the SNP distribution. We also ran generalized linear models across all 3 ranges to assess how haploblock allele frequency changed with absolute latitude, using range (North America, Europe, or Australia) and latitude as well as their interaction as fixed effects. Nonsignificant interactions were removed. Model estimates along with the 95% CI ribbons were plotted with the R package *emmeans* (Lenth et al. 2019).

Genome-wide Association

Of the 443 samples in this study, 226 had been measured in a common garden for multiple ecologically important phenotypes by van Boheemen, Atwater et al. (2019). We performed GWAS using 13 phenotypes: *floral sex allocation, flowering end, flowering onset, length of longest leaf, length of longest raceme, maximum height, pollen production end, number of racemes, root/shoot ratio, seed weight, shoot biomass, total biomass,* and *total reproductive biomass*. Three outlier sample measurements (>3 SD from the mean) were removed from the *length of longest leaf* phenotype. *Floral sex allocation* and *number of racemes* were respectively $\log_{10}$- and square root-transformed.

Beagle files for GWAS were generated in *angsd* v0.939 (Korneliussen et al. 2014) using the same parameters as the population structure analysis (-GL 2 -doMajorMinor 1 -doCounts 1 -doGLF 2 -SNP_pval 1e-6 -doMaf 2 -doGeno −1 -minMapQ 30 -minQ 20 -minMaf 0.05 -setMinDepthInd 2 -uniqueOnly 1 -doPlink 2) using only sites that could be estimated in >75% of samples (-minInd 170). Quantitative trait GWAS were performed in *angsd* v.0.939 (Korneliussen et al. 2014) (-yQuant -Pvalue 1 -doAsso 4). To avoid bias from population structure in our GWAS, we included the first two principal components of a genomic covariance matrix as covariates (-cov). The covariance matrix was generated with *pcangsd* v.1.2 (Meisner and Albrechtsen 2018) using the same parameters as the population structure analysis: a sample of 100,000 LD-pruned variants (*plink* v1.9 (Chang et al. 2015); −indep-pairwise 50 5 0.5) from outside annotated genes and haploblocks. GWAS results were analyzed in 10-kbp nonoverlapping windows across the genome using *The Weighted-Z Analysis* (*The WZA*; Booker et al. 2023).

GO and Flowering-Time Gene Enrichment

GO enrichment was assessed using functional annotations described in (Battlay et al. 2023). To identify GO terms enriched among candidate lists, the R package *topGO* (Alexa and Rahnenführer 2009) was used with Fisher's exact test, the "weight01" algorithm, and a P-value < 0.05 to assess significance. Following the recommendation in the *topGO* manual, we did not apply a multiple testing correction, as the "weight01" algorithm conditions P-values of GO terms on neighboring terms. In addition, we assessed enrichments of the 513 *A. artemisiifolia* genes that are orthologs of *A. thaliana* FLOR-ID flowering-time pathway genes (Bouché et al. 2016) using Fisher's exact test and a $P < 0.05$ threshold.

Trait Variance Partitioning

To partition trait variation into contributions from haploblocks versus the remaining polygenic background (Koch et al. 2022), we built a genomic relationship matrix (GRM) from 10,000 LD-thinned SNPs outside haploblocks using the R package *AGHMatrix* (Amadeu et al. 2023). We used SNPs from the 207 samples with both SNP and phenotype data available (supplementary table S1, Supplementary Material online), and made the matrix positive-definite by adding a small positive value (1×10^{-15}) to any eigenvalue smaller than 1×10^{-15} using the R package *mbend* (Nilforooshan 2020).

Next, we fitted a model to each trait in a Bayesian framework as implemented in the R package *MCMCglmm* (Hadfield 2010). Each model included genotypes of between 1 and 5 trait-associated haploblocks as fixed effects, and the GRM as a random effect to model the effect of additive genetic variation located outside haploblocks. We set a parameter-expanded prior on random effects ($V = 1$, N=2, a_μ=0, a_V= 1000) and an Inverse-Wishart prior ($V = 1$, N=0.002) on

residuals. 7,010,000 Markov chain Monte Carlo iterations were run with a thinning period of 7,000 iterations and a burn-in period of 10,000 iterations. Model parameters were estimated from their posterior distribution using 1,000 thinned iterations. Autocorrelations between MCMC samples were below the recommended level of 0.1, yielding effective sample sizes >753 for all estimates. We inspected plots of traces and posterior distributions to ensure that models converged. Other priors were explored and gave similar results to those presented here.

Last, we calculated the total variation of each trait as the sum of the variation explained by haploblocks (calculated following de Villemereuil et al. 2018), the additive genetic variation outside haploblocks, and the residual variation. We then calculated the proportion of total trait variation explained by each component, along with its 95% credible interval.

Local Adaptation Scans

For each sampling location, we extracted 19 bioclimatic variables from the WorldClim database (Fick and Hijmans 2017) using the R package *raster* (Hijmans et al. 2015), and selected four bioclimatic variables (BIO1: annual mean temperature; BIO2: mean diurnal range; BIO12: annual precipitation; BIO15: precipitation seasonality) that were minimally correlated ($r < 0.7$) in all three ranges for further analysis. We first generated beagle files in *angsd* v.0.939 (Korneliussen et al. 2014) (-GL 2 -doMajorMinor 1 -doCounts 1 -doGLF 2 -SNP_pval 1e-6 -doMaf 2 -doGeno −1 -minMapQ 30 -minQ 20 -minMaf 0.05 -setMinDepthInd 2 -uniqueOnly 1) in each range separately using all samples from populations with $n > 2$, and with the -minInd flag set to 75% of the number of samples per range. The resulting sites with range wide allele frequencies >0.05 were then measured in each population separately in subsequent *angsd* analyses (-doMaf 4 -minInd 2) with no minor allele frequency filter. The *BayPass* v.2.2 core model (Gautier 2015) (with an Ω covariance matrix computed from 10,000 randomly sampled sites that were located outside annotated genes and haploblocks) was run using population allele frequencies in each range separately. Correlations between population allele frequencies and the four independent bioclimatic variables were also measured in each range separately using τ (Kendall 1938). The results of *BayPass* XtX and τ correlations were further analyzed for enrichment in 10 kbp nonoverlapping windows across the genome using *The WZA* (Booker et al. 2023).

Contrast Scans

To identify regions of the genome that have been the target of divergent selection during range expansion, we used the BayPass contrast statistic (Olazcuaga et al. 2020) to compare population allele frequencies across each invaded range with source populations in the native North American range identified by our demographic analyses (Fig. 1; supplementary table S1, Supplementary Material online). We first generated beagle files in *angsd* v.0.939 (Korneliussen et al. 2014) (-GL 2 -doMajorMinor 1 -doCounts 1 -doGLF 2 -SNP_pval 1e-6 -doMaf 2 -doGeno −1 -minMapQ 30 -minQ 20 -minMaf 0.05 -setMinDepthInd 2 -uniqueOnly 1) in each combination of North American and European or Australian ranges. All samples from populations with $n > 2$ were included with the exception of Australia, where we excluded samples presumed to be part of a second, recent introduction (supplementary fig. S1, Supplementary Material online). For each analysis, the -minInd flag was set to 75% of the number of samples per range pair. The resulting sites that had frequencies of >0.05 across each range pair were then measured in each population separately with no minor allele frequency filter (-doMaf 4 -minInd 2). The *BayPass* v.2.2 contrast model (Olazcuaga et al. 2020) was run comparing population allele frequencies in North America with each of Europe and Australia separately using an Ω covariance matrix computed from 10,000 randomly sampled sites that were located outside annotated genes and haploblocks.

Contrast scans were conducted in BayPass for each invaded range separately using an omega matrix calculated from 10,000 putatively neutral sites to account for population structure. We assessed the enrichment of extreme contrast values in nonoverlapping 10 kbp windows using *The WZA* (Booker et al. 2023). To understand the source of divergence observed in contrast scans, we also scanned each range for evidence of selective sweeps. We calculated *H* (Fay and Wu 2000) with *angsd* v.0.939 (-doSaf 1 -doMajorMinor 4 -GL 2 -baq 2 -minMapQ 30 -minQ 20) using only sites that could be estimated in >75% of samples (-minInd), and the consensus of resequencing data from two outgroup species (*A. chamissonis* and *A. carduacea*; Bieker et al. 2022) mapped to the reference to determine the ancestral state at each site (-anc). *H* was calculated in 10 kbp nonoverlapping windows across the genome.

Supplementary Material

Supplementary material is available at *Molecular Biology and Evolution* online.

Acknowledgments

This research was supported by ARC Discovery Project grant DP220102362 awarded to K.A.H., A.F.-L. and J.R.S.

Author Contributions

Paul Battlay (Conceptualization, Data Curation, Formal Analysis, Methodology, Software, Visualization, Writing—Original Draft Preparation, Writing—Review & Editing), Samuel Craig (Formal Analysis, Software, Visualization, Writing—Original Draft Preparation), Andhika R. Putra (Formal Analysis, Investigation, Software, Writing—Original Draft Preparation), Keyne Monro (Formal Analysis, Investigation, Software, Writing—Original Draft Preparation), Nissanka P. De Silva (Formal Analysis, Investigation, Software, Writing—Original Draft Preparation), Jonathan Wilson (Formal Analysis, Software), Vanessa C. Bieker (Investigation), Saila Kabir (Investigation), Nawar Shamaya (Investigation), Lotte van Boheemen (Investigation), Loren H. Rieseberg (Resources), John R. Stinchcombe (Conceptualization, Funding Acquisition, Resources), Alexandre Fournier-Level (Conceptualization, Funding Acquisition, Resources, Supervision), Michael D. Martin (Conceptualization, Funding Acquisition, Resources, Supervision), Kathryn A. Hodgins (Conceptualization, Data Curation, Funding Acquisition, Methodology, Project Administration, Resources, Supervision, Writing—Review & Editing).

Data Availability

The diploid reference genome assembly used in this study is available from NCBI under BioProject IDs PRJNA929657 and PRJNA929658. Individual sample resequencing data are

available from ENA under BioProject IDs PRJEB48563, PRJNA339123, and PRJEB34825, and from SRA under BioProject ID PRJNA1139307. Phenotype data are available from github.com/lotteanna/traitclines. Code is available from github.com/pbattlay/ragweed-australia.

References

Alexa A, Rahnenführer J. Gene set enrichment analysis with topGO. *Bioconductor Improv*. 2009:27:1–26. https://bioconductor.org/packages/devel/bioc/vignettes/topGO/inst/doc/topGO.pdf.

Allendorf FW, Lundquist LL. Introduction: population biology, evolution, and control of invasive Species. *Conserv Biol*. 2003:17(1):24–30. https://doi.org/10.1046/j.1523-1739.2003.02365.x.

Amadeu RR, Garcia AAF, Munoz PR, Ferrão LFV. AGHmatrix: genetic relationship matrices in R. *Bioinformatics*. 2023:39(7):btad445. https://doi.org/10.1093/bioinformatics/btad445.

Angeloni F, Ouborg NJ, Leimu R. Meta-analysis on the association of population size and life history with inbreeding depression in plants. *Biol Conserv*. 2011:144(1):35–43. https://doi.org/10.1016/j.biocon.2010.08.016.

Arneth A, Liu J, Razzaque J, Zayas CN, Watson R, Baste I, Larigauderie A, Leadley P, Pascual U, Baptiste B, *et al*. 2019. Summary for policymakers of the global assessment report on biodiversity and ecosystem services of the Intergovernmental Science-Policy Platform on Biodiversity and Ecosystem Services-ADVANCE UNEDITED VERSION. [accessed 2024 May 7]. Available from: https://pesquisa.bvsalud.org/portal/resource/pt/biblio-1179448.

Baker HG, Stebbins GL. *Genetics of colonizing species*. New York: Academic Press; 1965.

Battey CJ, Ralph PL, Kern AD. Predicting geographic location from genetic variation with deep neural networks. *Elife*. 2020:9:e54507. https://doi.org/10.7554/eLife.54507.

Battlay P, Hendrickson BT, Mendez-Reneau JI, Santangelo JS, Albano LJ, Wilson J, Caizergues AE, King N, Puentes A, Tudoran A, *et al*. Structural variants underlie parallel adaptation following global invasion. *bioRxiv 602765*. https://doi.org/10.1101/2024.07.09.602765, 13 July 2024, preprint: not peer reviewed.

Battlay P, Wilson J, Bieker VC, Lee C, Prapas D, Petersen B, Craig S, van Boheemen L, Scalone R, de Silva NP, *et al*. Large haploblocks underlie rapid adaptation in the invasive weed *Ambrosia artemisiifolia*. *Nat Commun*. 2023:14(1):1717. https://doi.org/10.1038/s41467-023-37303-4.

Battlay P, Yeaman S, Hodgins KA. Impacts of pleiotropy and migration on repeated genetic adaptation. *Genetics*. 2024:228:iyae111. https://doi.org/10.1093/genetics/iyae111.

Bieker VC, Battlay P, Petersen B, Sun X, Wilson J, Brealey JC, Bretagnolle F, Nurkowski K, Lee C, Barreiro FS, *et al*. Uncovering the genomic basis of an extraordinary plant invasion. *Sci Adv*. 2022:8(34):eabo5115. https://doi.org/10.1126/sciadv.abo5115.

Bock DG, Caseys C, Cousens RD, Hahn MA, Heredia SM, Hübner S, Turner KG, Whitney KD, Rieseberg LH. What we still don't know about invasion genetics. *Mol Ecol*. 2015:24(9):2277–2297. https://doi.org/10.1111/mec.13032.

Booker TR, Yeaman S, Whiting JR, Whitlock MC. The WZA: a window-based method for characterizing genotype-environment associations. *Mol Ecol Resour*. 2023:24:e13768. https://doi.org/10.1111/1755-0998.13768.

Bouché F, Lobet G, Tocquin P, Périlleux C. FLOR-ID: an interactive database of flowering-time gene networks in *Arabidopsis thaliana*. *Nucleic Acids Res*. 2016:44(D1):D1167–D1171. https://doi.org/10.1093/nar/gkv1054.

Browning BL, Zhou Y, Browning SR. A one-penny imputed genome from next-generation reference panels. *Am J Hum Genet*. 2018:103(3):338–348. https://doi.org/10.1016/j.ajhg.2018.07.015.

Byrne D, Scheben A, Scott JK, Webber BL, Batchelor KL, Severn-Ellis AA, Gooden B, Bell KL. Genomics reveals the history of a complex plant invasion and improves the management of a biological invasion from the South African-Australian biotic exchange. *Ecol Evol*. 2022:12(8):e9179. https://doi.org/10.1002/ece3.9179.

Caillaud D, Thibaudon M, Martin S, Ségala C, Besancenot JP, Clot B, François H. Short-term effects of airborne ragweed pollen on clinical symptoms of hay fever in a panel of 30 patients. *J Investig Allergol Clin Immunol*. 2014:24:249–256. https://www.jiaci.org/summary/vol24-issue4-num1134.

Campbell MA, Anderson EC, Garza JC, Pearse DE. Polygenic basis and the role of genome duplication in adaptation to similar selective environments. *J Hered*. 2021:112(7):614–625. https://doi.org/10.1093/jhered/esab049.

Carøe C, Gopalakrishnan S, Vinner L, Mak SST, Sinding MHS, Samaniego JA, Wales N, Sicheritz-Pontén T, Gilbert MTP. Single-tube library preparation for degraded DNA. *Methods Ecol Evol*. 2018:9(2):410–419. https://doi.org/10.1111/2041-210X.12871.

Chang CC, Chow CC, Tellier LC, Vattikuti S, Purcell SM, Lee JJ. Second-generation PLINK: rising to the challenge of larger and richer datasets. *GigaScience*. 2015:4(1):7. https://doi.org/10.1186/s13742-015-0047-8.

Charlesworth B. Effective population size and patterns of molecular evolution and variation. *Nat Rev Genet*. 2009:10(3):195–205. https://doi.org/10.1038/nrg2526.

Chase MW, Hills HH. Silica gel: an ideal material for field preservation of leaf samples for DNA studies. *Taxon*. 1991:40(2):215–220. https://doi.org/10.2307/1222975.

Chauvel B, Dessaint F, Cardinal-Legrand C, Bretagnolle F. The historical spread of *Ambrosia artemisiifolia* L. In France from herbarium records. *J Biogeogr*. 2006:33(4):665–673. https://doi.org/10.1111/j.1365-2699.2005.01401.x.

Chevin L-M, Martin G, Lenormand T. Fisher's model and the genomics of adaptation: restricted pleiotropy, heterogenous mutation, and parallel evolution. *Evolution*. 2010:64(11):3213–3231. https://doi.org/10.1111/j.1558-5646.2010.01058.x.

Clavero M, García-Berthou E. Invasive species are a leading cause of animal extinctions. *Trends Ecol Evol*. 2005:20(3):110. https://doi.org/10.1016/j.tree.2005.01.003.

Collin F-D, Durif G, Raynal L, Lombaert E, Gautier M, Vitalis R, Marin J-M, Estoup A. Extending approximate Bayesian computation with supervised machine learning to infer demographic history from genetic polymorphisms using DIYABC random forest. *Mol Ecol Resour*. 2021:21(8):2598–2613. https://doi.org/10.1111/1755-0998.13413.

Conte GL, Arnegard ME, Peichel CL, Schluter D. The probability of genetic parallelism and convergence in natural populations. *Proc Biol Sci*. 2012:279(1749):5039–5047. https://doi.org/10.1098/rspb.2012.2146.

Danecek P, Auton A, Abecasis G, Albers CA, Banks E, DePristo MA, Handsaker RE, Lunter G, Marth GT, Sherry ST, *et al*. The variant call format and VCFtools. *Bioinformatics*. 2011:27(15):2156–2158. https://doi.org/10.1093/bioinformatics/btr330.

Della Torre F, Sala S, Sciancalepore L, Cassani L, Piazza G. Ragweed and allergy: epidemiology. *Allergy*. 1996:51:123.

DePristo MA, Banks E, Poplin R, Garimella KV, Maguire JR, Hartl C, Philippakis AA, del Angel G, Rivas MA, Hanna M, *et al*. A framework for variation discovery and genotyping using next-generation DNA sequencing data. *Nat Genet*. 2011:43(5):491–498. https://doi.org/10.1038/ng.806.

de Villemereuil P, Morrissey MB, Nakagawa S, Schielzeth H. Fixed-effect variance and the estimation of repeatabilities and heritabilities: issues and solutions. *J Evol Biol*. 2018:31(4):621–632. https://doi.org/10.1111/jeb.13232.

Dlugosch KM, Anderson SR, Braasch J, Cang FA, Gillette HD. The devil is in the details: genetic variation in introduced populations and its contributions to invasion. *Mol Ecol*. 2015:24(9):2095–2111. https://doi.org/10.1111/mec.13183.

Dlugosch KM, Parker IM. Founding events in species invasions: genetic variation, adaptive evolution, and the role of multiple introductions. *Mol Ecol*. 2008a:17(1):431–449. https://doi.org/10.1111/j.1365-294X.2007.03538.x.

Dlugosch KM, Parker IM. Invading populations of an ornamental shrub show rapid life history evolution despite genetic bottlenecks. *Ecol*

Lett. 2008b:11(7):701–709. https://doi.org/10.1111/j.1461-0248.2008.01181.x.
Dogantzis KA, Raffiudin R, Putra RE, Shaleh I, Conflitti IM, Pepinelli M, Roberts J, Holmes M, Oldroyd BP, Zayed A, *et al*. Post-invasion selection acts on standing genetic variation despite a severe founding bottleneck. *Curr Biol*. 2024:34(6):1349–1356.e4. https://doi.org/10.1016/j.cub.2024.02.010.
Doyle JJ, Doyle JL. A rapid DNA isolation procedure for small quantities of fresh leaf tissue. *Phytochem Bull*. 1987:19(1):11–15. https://worldveg.tind.io/record/33886/.
Dukes JS, Mooney HA. Does global change increase the success of biological invaders? *Trends Ecol Evol*. 1999:14(4):135–139. https://doi.org/10.1016/S0169-5347(98)01554-7.
Estoup A, Ravigné V, Hufbauer R, Vitalis R, Gautier M, Facon B. Is there a genetic paradox of biological invasion? *Annu Rev Ecol Evol Syst*. 2016:47(1):51–72. https://doi.org/10.1146/annurev-ecolsys-121415-032116.
Fauvergue X, Vercken E, Malausa T, Hufbauer RA. The biology of small, introduced populations, with special reference to biological control. *Evol Appl*. 2012:5(5):424–443. https://doi.org/10.1111/j.1752-4571.2012.00272.x.
Fay JC, Wu CI. Hitchhiking under positive Darwinian selection. *Genetics*. 2000:155(3):1405–1413. https://doi.org/10.1093/genetics/155.3.1405.
Fick SE, Hijmans RJ. WorldClim 2: new 1-km spatial resolution climate surfaces for global land areas. *Int J Climatol*. 2017:37(12):4302–4315. https://doi.org/10.1002/joc.5086.
Fisher RA. XV.—the correlation between relatives on the supposition of Mendelian inheritance. *Earth Environ Sci Trans R Soc Edinb*. 1919:52(2):399–433. https://doi.org/10.1017/S0080456800012163.
Fisher RA. *The genetical theory of natural selection*. Oxford, UK: The Clarendon Press; 1930.
Fokam E, Hashimoto S, Irshad R, Novitsky R, Allahverdiyev R, Mathur VB, Suh Y, Disclaimer YS. 2023. Summary for policymakers of the thematic assessment of invasive alien species and their control of the Intergovernmental Science-Policy Platform on Biodiversity and Ecosystem Services -ADVANCE UNEDITED VERSION-2. [accessed 2024 May 7]. https://apo.org.au/node/324159.
Fontaine MC, Labbé F, Dussert Y, Delière L, Richart-Cervera S, Giraud T, Delmotte F. Europe as a bridgehead in the worldwide invasion history of grapevine downy mildew, *Plasmopara viticola*. *Curr Biol*. 2021:31(10):2155–2166.e4. https://doi.org/10.1016/j.cub.2021.03.009.
Fox EA, Wright AE, Fumagalli M, Vieira FG. ngsLD: evaluating linkage disequilibrium using genotype likelihoods. *Bioinformatics*. 2019:35(19):3855–3856. https://doi.org/10.1093/bioinformatics/btz200.
Gautier M. Genome-wide scan for adaptive divergence and association with population-specific covariates. *Genetics*. 2015:201(4):1555–1579. https://doi.org/10.1534/genetics.115.181453.
Hadfield J. MCMC methods for multi-response generalized linear mixed models. *J Stat Softw*. 2010:33(2):1–22. https://doi.org/10.18637/jss.v033.i02.
Hämälä T, Gorton AJ, Moeller DA, Tiffin P. Pleiotropy facilitates local adaptation to distant optima in common ragweed (*Ambrosia artemisiifolia*). *PLoS Genet*. 2020:16(3):e1008707. https://doi.org/10.1371/journal.pgen.1008707.
He Z-Z, Stotz GC, Liu X, Liu J-J, Wang Y-G, Yang J, Li L-F, Zhang W-J, Nan P, Song Z-P. A global synthesis of the patterns of genetic diversity in endangered and invasive plants. *Biol Conserv*. 2024:291:110473. https://doi.org/10.1016/j.biocon.2024.110473.
Hijmans RJ, Van Etten J, Cheng J, Mattiuzzi M, Sumner M, Greenberg JA, Lamigueiro OP, Bevan A, Racine EB, Shortridge A, *et al*. Package "raster". *R package*. 2015:734. https://rspatial.org/raster/pkg/RasterPackage.pdf.
Ivanova NV, Fazekas AJ, Hebert PDN. Semi-automated, membrane-based protocol for DNA isolation from plants. *Plant Mol. Biol. Rep*. 2008:26(3):186. https://doi.org/10.1007/s11105-008-0029-4.
Kendall MG. A new measure of rank correlation. *Biometrika*. 1938:30(1-2):81–93. https://doi.org/10.1093/biomet/30.1-2.81.
Kirkpatrick M, Barrett B. Chromosome inversions, adaptive cassettes and the evolution of species' ranges. *Mol Ecol*. 2015:24(9):2046–2055. https://doi.org/10.1111/mec.13074.
Kirkpatrick M, Barton N. Chromosome inversions, local adaptation and speciation. *Genetics*. 2006:173(1):419–434. https://doi.org/10.1534/genetics.105.047985.
Koch EL, Ravinet M, Westram AM, Johannesson K, Butlin RK. Genetic architecture of repeated phenotypic divergence in littorina saxatilis ecotype evolution. *Evolution*. 2022:76(10):2332–2346. https://doi.org/10.1111/evo.14602.
Korneliussen TS, Albrechtsen A, Nielsen R. ANGSD: analysis of next generation sequencing data. *BMC Bioinformatics*. 2014:15(1):356. https://doi.org/10.1186/s12859-014-0356-4.
Lenth R, Singmann H, Love J, Buerkner P, Herve M. 2019. Package "emmeans." https://cran.r-project.org/web/packages/emmeans/index.html.
Li H. Minimap2: pairwise alignment for nucleotide sequences. *Bioinformatics*. 2018:34(18):3094–3100. https://doi.org/10.1093/bioinformatics/bty191.
Li H. Aligning sequence reads, clone sequences and assembly contigs with BWA-MEM. *arXiv 3997*. https://doi.org/10.48550/arXiv.1303.3997, 26 May 2013, preprint: not peer reviewed.
Li H, Ralph P. Local PCA shows how the effect of population structure differs along the genome. *Genetics*. 2019:211(1):289–304. https://doi.org/10.1534/genetics.118.301747.
Li X-M, She D-Y, Zhang D-Y, Liao W-J. Life history trait differentiation and local adaptation in invasive populations of *Ambrosia artemisiifolia* in China. *Oecologia*. 2015:177(3):669–677. https://doi.org/10.1007/s00442-014-3127-z.
Liu C, Wolter C, Xian W, Jeschke JM. Most invasive species largely conserve their climatic niche. *Proc Natl Acad Sci U S A*. 2020:117(38):23643–23651. https://doi.org/10.1073/pnas.2004289117.
Ma L-J, Cao L-J, Chen J-C, Tang M-Q, Song W, Yang F-Y, Shen X-J, Ren Y-J, Yang Q, Li H, *et al*. Rapid and repeated climate adaptation involving chromosome inversions following invasion of an insect. *Mol Biol Evol*. 2024:41(3):msae044. https://doi.org/10.1093/molbev/msae044.
Marchini GL, Sherlock NC, Ramakrishnan AP, Rosenthal DM, Cruzan MB. Rapid purging of genetic load in a metapopulation and consequences for range expansion in an invasive plant. *Biol Invasions*. 2016:18(1):183–196. https://doi.org/10.1007/s10530-015-1001-5.
McDonough Y, Connallon T. Effects of population size change on the genetics of adaptation following an abrupt change in environment. *Evolution*. 2023:77(8):1852–1863. https://doi.org/10.1093/evolut/qpad103.
McGoey BV, Hodgins KA, Stinchcombe JR. Parallel flowering time clines in native and introduced ragweed populations are likely due to adaptation. *Ecol Evol*. 2020:10(11):4595–4608. https://doi.org/10.1002/ece3.6163.
McGoey BV, Stinchcombe JR. Introduced populations of ragweed show as much evolutionary potential as native populations. *Evol Appl*. 2021:14(5):1436–1449. https://doi.org/10.1111/eva.13211.
Meisner J, Albrechtsen A. Inferring population structure and admixture proportions in low-depth NGS data. *Genetics*. 2018:210(2):719–731. https://doi.org/10.1534/genetics.118.301336.
Meyer M, Kircher M. Illumina sequencing library preparation for highly multiplexed target capture and sequencing. *Cold Spring Harb Protoc*. 2010:2010(6):db.prot5448. https://doi.org/10.1101/pdb.prot5448.
Nadachowska-Brzyska K, Konczal M, Babik W. Navigating the temporal continuum of effective population size. *Methods Ecol Evol*. 2022:13(1):22–41. https://doi.org/10.1111/2041-210X.13740.
Nei M, Maruyama T, Chakraborty R. The bottleneck effect and genetic variability in populations. *Evolution*. 1975:29(1):1–10. https://doi.org/10.2307/2407137.
Nielsen R, Korneliussen T, Albrechtsen A, Li Y, Wang J. SNP calling, genotype calling, and sample allele frequency estimation from new-generation sequencing data. *PLoS One*. 2012:7(7):e37558. https://doi.org/10.1371/journal.pone.0037558.

Nilforooshan MA. Mbend: an R package for bending non-positive-definite symmetric matrices to positive-definite. *BMC Genet*. 2020:21(1):97. https://doi.org/10.1186/s12863-020-00881-z.

Novo I, Ordás P, Moraga N, Santiago E, Quesada H, Caballero A. Impact of population structure in the estimation of recent historical effective population size by the software GONE. *Genet Sel Evol*. 2023:55(1):86. https://doi.org/10.1186/s12711-023-00859-2.

Olazcuaga L, Loiseau A, Parrinello H, Paris M, Fraimout A, Guedot C, Diepenbrock LM, Kenis M, Zhang J, Chen X, *et al*. A whole-genome scan for association with invasion success in the fruit fly *Drosophila suzukii* using contrasts of allele frequencies corrected for population structure. *Mol Biol Evol*. 2020:37(8):2369–2385. https://doi.org/10.1093/molbev/msaa098.

Orr HA. The population genetics of adaptation: the distribution of factors fixed during adaptive evolution. *Evolution*. 1998:52(4):935–949. https://doi.org/10.2307/2411226.

Parsons WT, Cuthbertson EG. *Noxious weeds of Australia*. Clayton, Victoria, Australia: Csiro Publishing; 2001.

Pejchar L, Mooney H. The impact of invasive alien species on ecosystem services and human well-being. *Trends Ecol Evol*. 2010:24(9):161–182. https://doi.org/10.1093/acprof:oso/9780199560158.003.0012.

Pimentel D, Zuniga R, Morrison D. Update on the environmental and economic costs associated with alien-invasive species in the United States. *Ecol Econ*. 2005:52(3):273–288. https://doi.org/10.1016/j.ecolecon.2004.10.002.

Prapas D, Scalone R, Lee J, Nurkowski KA, Bou-Assi S, Rieseberg L, Battlay P, Hodgins KA. Quantitative trait loci mapping reveals an oligogenic architecture of a rapidly adapting trait during the European invasion of common ragweed. *Evol Appl*. 2022:15(8):1249–1263. https://doi.org/10.1111/eva.13453.

Putra AR, Hodgins KA, Fournier-Level A. Assessing the invasive potential of different source populations of ragweed (*Ambrosia artemisiifolia* L.) through genomically informed species distribution modelling. *Evol Appl*. 2023:17:e13632. https://doi.org/10.1111/eva.13632.

Ralph PL, Coop G. The role of standing variation in geographic convergent adaptation. *Am Nat*. 2015:186(S1):S5–S23. https://doi.org/10.1086/682948.

Roesti M, Gilbert KJ, Samuk K. Chromosomal inversions can limit adaptation to new environments. *Mol Ecol*. 2022:31(17):4435–4439. https://doi.org/10.1111/mec.16609.

Rohland N, Reich D. Cost-effective, high-throughput DNA sequencing libraries for multiplexed target capture. *Genome Res*. 2012:22(5):939–946. https://doi.org/10.1101/gr.128124.111.

Santangelo JS, Ness RW, Cohan B, Fitzpatrick CR, Innes SG, Koch S, Miles LS, Munim S, Peres-Neto PR, Prashad C, *et al*. Global urban environmental change drives adaptation in white clover. *Science*. 2022:375(6586):1275–1281. https://doi.org/10.1126/science.abk0989.

Schrieber K, Lachmuth S. The genetic paradox of invasions revisited: the potential role of inbreeding × environment interactions in invasion success. *Biol Rev Camb Philos Soc*. 2017:92(2):939–952. https://doi.org/10.1111/brv.12263.

Schubert M, Ermini L, Der Sarkissian C, Jónsson H, Ginolhac A, Schaefer R, Martin MD, Fernández R, Kircher M, McCue M, *et al*. Characterization of ancient and modern genomes by SNP detection and phylogenomic and metagenomic analysis using PALEOMIX. *Nat Protoc*. 2014:9(5):1056–1082. https://doi.org/10.1038/nprot.2014.063.

Schubert M, Lindgreen S, Orlando L. AdapterRemoval v2: rapid adapter trimming, identification, and read merging. *BMC Res Notes*. 2016:9(1):88. https://doi.org/10.1186/s13104-016-1900-2.

Seebens H, Blackburn TM, Dyer EE, Genovesi P, Hulme PE, Jeschke JM, Pagad S, Pyšek P, Winter M, Arianoutsou M, *et al*. No saturation in the accumulation of alien species worldwide. *Nat Commun*. 2017:8(1):14435. https://doi.org/10.1038/ncomms14435.

Sherpa S, Després L. The evolutionary dynamics of biological invasions: a multi-approach perspective. *Evol Appl*. 2021:14(6):1463–1484. https://doi.org/10.1111/eva.13215.

Simons YB, Sella G. The impact of recent population history on the deleterious mutation load in humans and close evolutionary relatives. *Curr Opin Genet Dev*. 2016:41:150–158. https://doi.org/10.1016/j.gde.2016.09.006.

Skotte L, Korneliussen TS, Albrechtsen A. Estimating individual admixture proportions from next generation sequencing data. *Genetics*. 2013:195(3):693–702. https://doi.org/10.1534/genetics.113.154138.

Tepolt CK, Palumbi SR. Rapid adaptation to temperature via a potential genomic island of divergence in the invasive green crab, *Carcinus maenas*. *Front Ecol Evol*. 2020:8:580701. https://doi.org/10.3389/fevo.2020.580701.

Uller T, Leimu R. Founder events predict changes in genetic diversity during human-mediated range expansions. *Glob Chang Biol*.2011:17(11):3478–3485. https://doi.org/10.1111/j.1365-2486.2011.02509.x.

van Boheemen LA, Atwater DZ, Hodgins KA. Rapid and repeated local adaptation to climate in an invasive plant. *New Phytol*. 2019:222(1):614–627. https://doi.org/10.1111/nph.15564.

van Boheemen LA, Bou-Assi S, Uesugi A, Hodgins KA. Rapid growth and defence evolution following multiple introductions. *Ecol Evol*. 2019:9(14):7942–7956. https://doi.org/10.1002/ece3.5275.

van Boheemen LA, Hodgins KA. Rapid repeatable phenotypic and genomic adaptation following multiple introductions. *Mol Ecol*. 2020:29(21):4102–4117. https://doi.org/10.1111/mec.15429.

van Boheemen LA, Lombaert E, Nurkowski KA, Gauffre B, Rieseberg LH, Hodgins KA. Multiple introductions, admixture and bridgehead invasion characterize the introduction history of *Ambrosia artemisiifolia* in Europe and Australia. *Mol Ecol*. 2017:26(20):5421–5434. https://doi.org/10.1111/mec.14293.

Van der Auwera GA, O'Connor BD. *Genomics in the cloud: using docker, GATK, and WDL in terra*. Sebastopol, CA, USA: O'Reilly Media, Inc.; 2020.

Westram AM, Faria R, Johannesson K, Butlin R, Barton N. Inversions and parallel evolution. *Philos Trans R Soc Lond B Biol Sci*. 2022:377(1856):20210203. https://doi.org/10.1098/rstb.2021.0203.

Whitlock MC, Davis B. Genetic load. *eLS*. 2011:2. https://doi.org/10.1002/9780470015902.a0001787.pub2

Willi Y, Griffin P, Van Buskirk J. Drift load in populations of small size and low density. *Heredity (Edinb)*. 2013:110(3):296–302. https://doi.org/10.1038/hdy.2012.86.

Willi Y, Van Buskirk J, Hoffmann AA. Limits to the adaptive potential of small populations. *Annu Rev Ecol Evol Syst*. 2006:37(1):433–458. https://doi.org/10.1146/annurev.ecolsys.37.091305.110145.

Wilson J, Bieker VC, van Boheemen L, Connallon T, Martin MD, Battlay P, Hodgins KA. In press. Copy number variation contributes to parallel local adaptation in an invasive plant. *PNAS*. [accepted 2025 Jan 3]. https://doi.org/10.1101/2024.07.03.601998.

Yeaman S, Gerstein AC, Hodgins KA, Whitlock MC. Quantifying how constraints limit the diversity of viable routes to adaptation. *PLoS Genet*. 2018:14(10):e1007717. https://doi.org/10.1371/journal.pgen.1007717.

Yeaman S, Whitlock MC. 2011. The genetic architecture of adaptation under migration-selection balance. *Evolution*. 65(7):1897–1911. https://doi.org/10.1111/j.1558-5646.2011.01269.x.